Proceedings of the ASME 27th International Conference on Offshore Mechanics and Arctic Engineering
OMAE2008
June 15-20, 2008, Estoril, Portugal

OMAE2008-57045

REYNOLDS NUMBER DEPENDENCE OF FLEXIBLE CYLINDER VIV RESPONSE DATA

Susan B. Swithenbank
Center for Ships and Ocean Structures
Department of Marine Technology
Norwegian University of Science and Technology

J. Kim Vandiver
Department Mechanical Engineering
Massachusetts Institute of Technology

Carl Martin Larsen
Center for Ships and Ocean Structures
Department of Marine Technology
Norwegian University of Science and Technology

Halvor Lie
MARINTEK

ABSTRACT

The response amplitude and the non-dimensional frequency of flexible cylinder vortex-induced vibrations from laboratory and field experiments show significant trends with increasing Reynolds number from 10^3 to $2*10^5$. The analysis uses complex data from experiments with wide variations in the physical parameters of the system, including length-to-diameter ratios from 82 to 4236, tension dominated natural frequencies and bending stiffness dominated natural frequencies, sub-critical and critical Reynolds numbers, different damping coefficients, standing wave and traveling wave vibrations, mode numbers from $1-25^{th}$, and different mass ratios.

1 Introduction

The Reynolds number, Re, is an important parameter in Vortex-Induced Vibrations (VIV).

$$Re = \frac{UD}{\upsilon} \tag{1}$$

U is the current velocity, D is the diameter, and υ is the kinematic viscosity. Sarpkaya (2004) provides a discussion of the effects of Reynolds number on VIV. The majority of the test data discussed by Sarpkaya is at Reynolds numbers between 500 and $6*10^4$ which is lower than the majority of the tests analyzed here. Sarpkaya notes that in the Reynolds number range of 10^3 to $2*10^5$, which is of interest to this study, includes the smooth transition of the Strouhal number, a decrease in wake width with a corresponding reduction in drag coefficient, and the lack of 2P and 2S shedding modes.

Bearman (1984) discusses the effect of Reynolds number on the correlation length in two-dimensional flow experiments. He also discusses other factors such as body-surface finish, aspect ratio, end-plate design, flow turbulence, blockage ratio and acoustic noise level.

Blevins (2001) shows that the composition of the vortex pattern from the bluff body will change depending on Reynolds number. The experiments examined here are in the regime where the vortex street is the fully turbulent and include examples up to a Reynolds number of $3*10^5$.

Khalak & Williamson (1997) show that the amplitude of vibration for flexible cylinders is effected by the reduced

velocity, V_{rn}.

$$V_{rn} = \frac{U}{f_n * D} \tag{2}$$

where f_n is the natural frequency in air. They defined three separate regimes with an initial branch with increasing amplitudes, an upper branch with peak amplitudes and lower branch with decreasing amplitudes.

In rigid cylinders with very low damping, Govardhan & Williamson (2006) show that the peak response amplitude is dependent on Reynolds number over a narrow range of reduced velocities. They show a linear increase in peak response amplitude versus the logarithm base ten of the Reynolds number which is approximated by the expression:

$$\frac{A}{D} = log(0.41Re^{0.36}) \tag{3}$$

where A is the peak amplitude of vibration. The work of this paper was inspired by the work of Govardhan & Williamson (2006). Originally this research was undertaken to see if a similar relationship would be found in flexible cylinder data.

Other important parameters when studying VIV include the non-dimensional frequency, $\hat{f}$, and the mass ratio, m*.

$$\hat{f} = \frac{f_v D}{U} \tag{4}$$

$$m^* = \frac{m}{\frac{\pi}{4}\rho_f D^2} \tag{5}$$

where f_v is the frequency of vibration for the individual test run, m is the mass per unit length and ρ_f is the density of the fluid. Govardhan & Williamson (2000) show that as mass ratio decreases there is an increase in the range of V_{rn} over which large amplitude vibrations exist. Further they show that the range of synchronization for the upper branch of response increases with a decrease in mass ratio.

2 Experimental Data

The tests analyzed here were taken from both laboratory experiments and ocean experiments. All of these experiments have some key parameters in common such as the pinned-pinned boundary conditions and structural damping ratios of less than 1%. The other physical parameters such as length-to-diamter ratio, mode number and Reynolds number vary significantly between the different experiments. The majority of the tests were done in laboratory tanks with low turbulence levels. The exception to low turbulence was the Gulf Stream test where moderate turbulence levels were present in the ocean environment. For this analysis, the temperature dependent kinematic viscosities were used.

Below is an list of the experiments analyzed in this paper. Key parameters are summarized in Table 1. For each experiment, the table contains the length-to-diameter ratio, the range of Reynolds numbers, the tension (T), the mass ratio (m*), the range of dominant cross-flow mode numbers (n), and the symbol used to represent that test in later figures (Sym).

- The High-Mode tests were conducted in the Ocean Basin at Marintek, using a 38m flexible pipe with 0.027 m diameter. These tests were done in uniform and linear shear flows and excited up to the 16^{th} mode for the dominant cross-flow VIV. (Trim et al., 2005)
- The Lake Seneca tests were conducted at the Naval Surface Warfare Center acoustic test facility at Lake Seneca, New York on a 122.2 m pipe with 0.033 m diameter. These tests were designed to excite from 10^{th} to 25^{th} mode cross-flow in uniform flow VIV. (Vandiver et al., 2005)
- The Rotating Rig tests were conducted in the tow tank at Marintek on a cylinder of length 11.34 m. The tests were designed to evaluate the effects of staggered buoyancy on the riser. Two different configurations of the rotating rig were used for this analysis, the bare pipe with a diameter of 0.02 m and the full buoyancy coverage of the cylinder with a diameter of 0.05 m. Both uniform flow and linearly shear tests were conducted and used for this analysis. (Lie, Mo & Vandiver, 1998)
- The Steel Catenary Riser (SCR) tests were conducted in the tow tank at Marintek. These tests were conducted with a high tension and high mass ratio. The pipe had a length of 28.342 m and a 0.023 m diameter and was towed in the catenary plane. The pipe used in these tests was curved with respect to the flow as in a typical SCR configuration, therefore all of the data was not linearly sheared flow because of the curvature of the pipe. For the SCR tests, the maximum velocity used in this paper was the maximum normal incident current taking into account the pipe curvature. (Halse et al., 1999)

• The Fairing Tests were conducted in the tow tank at Marintek on a cylinder of length 9.324 m and diameter of 0.02 m. The uniform flow tests were designed to analyze fairings with different length-to-cord ratios but only the bare cylinder data was used for this analysis. (Braaten, Lie & Skaugset, 2008)

• The Hangøytangen tests were conducted alongside a quay in Hangøytangen, Norway. The steel pipe was 90 m long and had a diameter of 0.03 m. These tests were linearly varying sheared flow tests. The Hangøytangen tests were unique because they had both bending stiffness controlled natural frequencies as well as tension dominated natural frequencies. (Huse, Kleiven, & Nielsen, 1998)

• The Gulf Stream Tests were conducted in 2006 by MIT in the Gulf Stream near Miami, Florida aboard the Research Vessel F. G. Walton Smith from the University of Miami. This experiment tested a 152.5 m cylinder with a 0.036 m diameter. These tests were conducted in naturally occurring uniform and sheared flow. (Vandiver et al., 2006)

• The Long Tensioned Risers tests were conducted at Skibsteknisk Laboratories in Denmark in 1981. Four different test conditions were carried out that varied the tension and the mass per unit length of the aluminum riser which measured 9.93m long with a diameter of 0.12m. (Vandiver, 1993)

• The Castine experiments were conducted in the summer of 1981 in Castine, Maine. The experiments used a steel pipe that was strung between pilings on a sandbar. The incoming and outgoing tides submerged the sandbar provided a nearly uniform flow over the pipe. The pipe was 0.041 m in diameter and 22.86 m long. (Vandiver, 1983)

3 Analysis

In VIV experiments, more than one resonant frequency can be excited in the pipe at different times through the course of a single test run, especially for the experiments at high mode number and experiments with highly sheared current profiles, (Swithenbank, 2007). As the frequencies switch, the amplitude of vibration will decrease and then increase again at the new frequency. These experiments can exhibit vast changes in the amplitude of vibration over the duration of a single test. Thus, the Root Mean Squared (RMS) in time with the mean removed is a parameter for presenting the data that takes into account the high level of variation in amplitude at each sensor.

For a standing wave the measure amplitude will depend strongly on the sensor's location and its proximity to nodes or anti-nodes. For high mode number experiments with large length-to-diameter ratios, high amplitudes are seen in the power-in region, which is defined as the section of the cylinder where energy enters the system. There are many traveling waves with diminishing amplitudes as they propagate away from the power-in region (Marcollo et al., 2007).

To account for all of these variations, the RMS in time for each location was calculated and then averaged over all the locations. The mean RMS displacement, $\overline{\sigma}_{(y/D)}$, is given by:

$$\overline{\sigma}_{(y/D)} = \frac{\sum_{i=1}^{N} \sqrt{\frac{1}{M}\sum_{j=1}^{M}(y_j - \bar{y})_i^2}}{N * D} \tag{6}$$

where M is the number of samples, N is the number of sensors recorded in the test run, y_j is the j^{th} time step for a time series for an individual sensor, and $\bar{y}$ is the temporal mean of the time series. This metric allows for comparison of complex and different data sets.

Another metric used to compare the data in this paper is the maximum RMS. The RMS with the mean removed is taken in time at each location, then the location with the maximum RMS response is chosen. Especially when looking at high length-to-diameter ratios the maximum RMS may be more representative of the true dynamics of the system because the maximum RMS is normally found in the power-in region. In these high length-to-diameter ratio tests, damping will control the response outside the power-in region which is not representative of the dynamic response to VIV.

For the majority of the tests, the displacements were calculated from accelerometer data that was twice integrated in the time domain using a process described in Swithenbank (2007). A high-pass filter was necessary when integrating the data to prevent low-frequency noise expansion. An elliptical filter was used with a high pass cut-off value of $0.05 * U/D$ Hz.

The Hangøytangen and Gulf Steam tests used strain gages as sensors instead of accelerometers. The sensors did not have adequate spacial resolution to double integrate the signals in space, therefore accurate displacements were more difficult to determine. For the Hangøytangen tests modal analysis was done to estimate the displacement of the riser used in this analysis. The modal analysis introduces some error into the calculations and the reported displacements may be slightly lower than the true displacement, (Lie & Kaasen, 2006).

For the Gulf Stream experiment the phase velocity, c, of traveling waves was calculated from the measured phase lag between sensors. It varied from 30 to 40 m/s. The form $y(x,t) = Asin(\omega t \pm kx)$ was assumed for the traveling wave,

Test Name	L/D	Re	T(N)	m*	n	Sym
High Mode	1407.4	7.1e3 - 5.7e4	6000	1.76	1-16	○
Lake Seneca	3703.0	7.6e3 - 2.5e4	3225	1.31	10-25	□
Rot. Rig bare	567	3.5e3 - 2.8e4	713-1001	1.46	1-5	✡
Rot. Rig full	226.8	8.8e3 - 7.0e4	713-1001	1.12	1-5	♢
SCR	1232.3	1.6e3 - 2.9e4	241.2	2.28	1-9	△
Fairing	457.2	1.8e3 - 5.3e4	672-745	1.65	1-6	+
Hangøytangen	3000	3.7e3 - 2.6e4	3801	3.10	1-16	▽
Gulf Stream	4236.1	3.6e3 - 3.4e4	3225	1.18	10-25	◁
Tension Risers	82.75	1.1e4 - 2.4e5	16.7k-25.4k	1	1	⋆
Castine	557.6	2.6e4	1423-2669	2.4	1-3	*

Table 1. Experimental key parameters

where ω where is the frequency in radians per second and the wavenumber, k, is ω/c. Then, the RMS A/D was computed from the measured total RMS strain associated with the VIV response frequency, which includes the contributions of spectral components within plus or minus 10% of the dominant VIV cross-flow response frequency. If we define as the mean square measured strain in the two orthogonal bending planes of the test cylinder in the frequency band at the VIV frequency, then the estimated RMS displacement to diameter ratio is given by

$$\frac{A_{rms}}{D} = \frac{c^2}{RD\omega^2}\sqrt{\varepsilon_x^2 + \varepsilon_y^2} \tag{7}$$

where R is the radial distance of the strain gages from the neutral axis of the cylinder. This formula is used to compute the displacements for the Gulf Stream tests shown in this paper.

For the Long Tensioned Riser test and the Castine test, no time series were available for analysis. Instead the maximum RMS displacement and mode number were recorded in Vandiver (1993) and Mazel (1976) respectively. If sinusoidal mode shapes are assumed, then to get the mean RMS displacement the mode shapes are integrated and then divided by the length:

$$\overline{\sigma}_{(y/D)} = \frac{y}{D}\frac{\int_0^L |sin\,(kx)|\,dx}{L} = \frac{2}{\pi}\frac{y}{D} \tag{8}$$

where y is the RMS cross-flow amplitude at the anti-node and k is the wavenumber.

For both the SCR data and the Lake Seneca data, the alignment of the sensors did not match exactly with the cross-flow and in-line vibrations. For these two tests a simple rotation matrix was used to rotate the two orthogonal signals at one degree increments. At each incremental step, a Power Spectral Density (PSD) of the displacement time series was computed. The PSD that maximized the peak cross-flow response at each sensor at the shedding frequency was used to identify the correct rotation angle, θ to be used at each location.

One question in analyzing the sheared data is which velocity is associated with the observed cross-flow vibration frequency. This velocity is needed to calculate the Reynolds number. The High Mode Data conducted experiments with the same current speeds in uniform flow and linear-shear profiles. When the response frequency from the sheared flow case frequency is divided by response frequency for the uniform flow case with the same maximum speed, the average of this value over all cases is 0.84. The value of 0.84 derived here is best for linear shear profiles like the High Mode Data, and will be less accurate for arbitrary profiles like the Gulf Stream experiments. For this analysis, a factor of 0.84 times the maximum current speed is used to specify the velocity for the sheared current profiles.

4 Non-Dimensional Frequency

The cross-flow non-dimensional frequencies are shown in Figure 1. The legend for the symbols is in Table 1. The dark blue points represent the uniform flow cases, while the cyan (light blue) points are the sheared

flow cases. The non-dimensional frequency starts at 0.22 for a Reynolds number of 10^3 and approaches 0.14 for Reynolds number of 10^5. The sheared flow cases, represent the largest scatter in the data. The non-dimensional frequencies for in-line were at twice the frequency of the cross-flow.

Similar trends are seen in the Strouhal Number graph from fixed cylinder experiments in Tropea, Yarin & Foss (2007). This shows similar trends with a decrease in Strouhal number for a Reynolds number range of 10^3 to 10^5. The largest variation in Figure 1 is from the sheared flow experiments where the exact excitation velocity is unknown.

5 Results

The mean RMS and the maximum RMS for each experiment are shown in Figure 2 with the legend shown in Table 1. The dark blue symbols represent the cross-flow uniform flow experiments, while the cyan symbols are the cross-flow sheared flow experiments. The red symbols are the in-line uniform flow experiments, while the magenta symbols are the in-line sheared flow cases. The solid lines are the least-square exponential fits to the cross-flow and in-line data respectively, with the dotted lines bracketing them representing plus and minus one standard deviation from the fitted curve. The upper dashed black line is the line derived by Govardhan & Williamson (2006) for rigid cylinders which was multiplied by a factor of $\sqrt{2}/2$ to get the RMS and by a factor of $2/\pi$ to get the spacial mean. These factors are so that the Govardhan & Williamson (2006) original peak data can be compared to the mean RMS data. In the top of Figure 2 bottom, Equation 3 has been multiplied by a factor of $\sqrt{2}/\pi$ and is represented by the dashed line. In the bottom of Figure 2, Equation 3 has been multiplied by a factor of $\sqrt{2}/2$ do get the RMS and is shown by a dashed line.

The least-square fit curves for the mean RMS cross-flow, mean RMS in-line, and maximum RMS cross-flow displacements respectively are:

$$\frac{y_{mean}}{D} = log(Re)^{0.168} - 0.328 \tag{9}$$

$$\frac{x_{mean}}{D} = log(Re)^{0.086} - 0.257 \tag{10}$$

$$\frac{y_{max}}{D} = log(Re)^{0.312} - 0.805 \tag{11}$$

Each least-square fit shows a clear trend of increasing amplitude-to-diameter, A/D, ratio with increasing Reynolds number for both the mean RMS and maximum RMS displacements.

Many different reasons contribute to the high scatter seen in the data:

- The precise velocity for the shear flow cases that excites the vibrations is unknown. For this analysis a value of 0.84 times U_{max} was used.
- In the low mode number tests, a small change in velocity could lead to a large change in the normalized displacement, because there is only a small range of reduced velocities where large amplitude vibrations are observed, as seen in the SCR test.
- A significant source of variation in the data is statistical. In some tests, the spatial resolution in sensor measurements was sparse. Equation 6 gives a coarse statistical measure of the response. Furthermore, most flexible cylinder experiments with high length-to-diameter ratios exhibit traveling waves which are largest in amplitude near the power-in region and attenuate with distance traveled. This was not accounted for in the top of Figure 2. The maximum RMS displacement as seen in the bottom of Figure 2 may not be at the maximum displacement of the pipe, depending on the placement of sensors relative to nodes and anti-nodes.
- In high-mode number tests, often more than one mode can be excited by any given current profile. As the frequency shifts from one frequency to another the amplitude decreases and then increases again, (Swithenbank, 2007). Since the RMS of each sensor has been taken in time, the shifting of the responding frequency leads to a lower time-averaged RMS displacement.
- The damping in Govardhan & Williamson (2006) was a well-characterized phenomenon with a known value. For many of the flexible cylinder experiments shown here, the effect of hydrodynamic damping outside the power-in region is unknown and decreases the amplitude of vibration causing more scatter in the data. Shear flow experiments and large length-to-diameter ratio experiments have finite power-in regions; in these cases, the hydrodynamic damping outside of the power-in region can be dominant (Vikestad, Larsen, & Vandiver, 2000).

6 Effects on Amplitude

Under stationary uniform flow conditions the lock-in A/D of a spring-mounted cylinder is dependent on three parameters: the lift coefficient, the response frequency, and

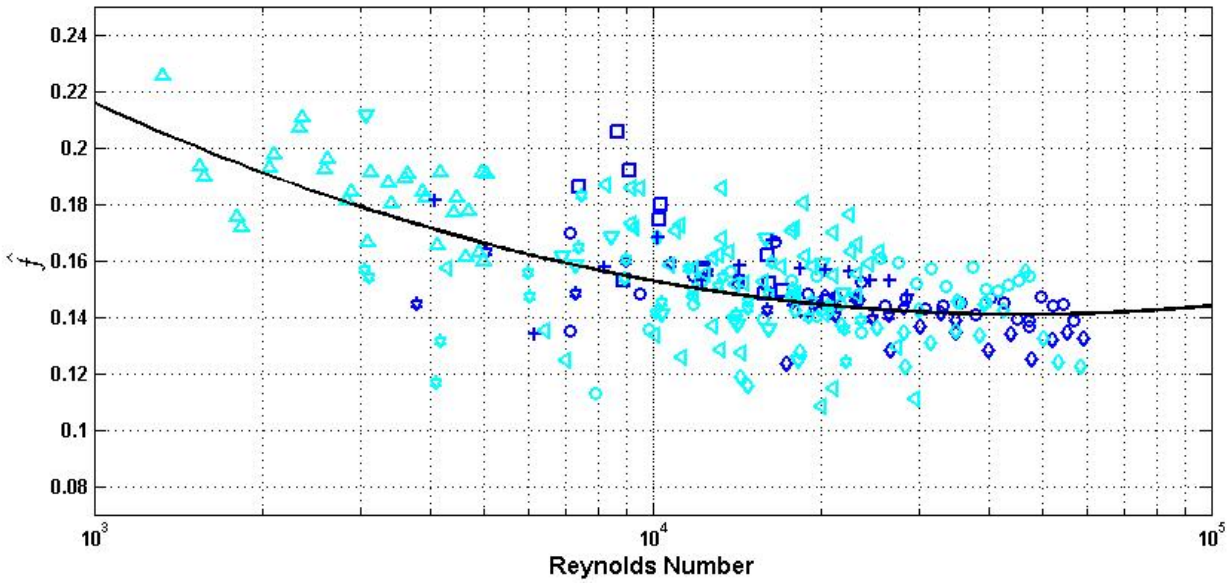

Figure 1. The non-dimensional frequency versus Reynolds number for uniform (blue) and shear flow (cyan) cases. Legend for the symbols in Table 1.

the current speed. This can be seen from the equation of motion for the cylinder:

$$m\ddot{y} + C\dot{y} + Ky = \frac{1}{2}\rho_f D U^2 C_L sin(\omega t) \tag{12}$$

where C is the damping constant, K is the spring force per unit displacement, C_L is the lift coefficient and ω is the frequency of oscillation. The displacement is assumed to have the form of $Acos(\omega t)$ since it can be approximated as a sinusoidal process. At resonance the inertia term and the stiffness term must cancel, therefore the input force must be balanced by the damping force and Equation 12 reduces to:

$$AC\omega = \frac{1}{2}\rho_f D U^2 C_L \tag{13}$$

Blevins (2001) shows that the lift coefficient C_L for stationary cylinders is Reynolds Number dependent. The results shown for flexible cylinders also are influenced by the Reynolds number. However, it is not only the magnitude of C_L that is important, but also the relationship between C_L and the response amplitude. By rearranging Equation 13, the A/D reduces to:

$$\frac{A}{D} = \frac{\rho_f U^2 C_L}{4\pi f C} \tag{14}$$

The experiments of Gopalkrishnan (1993) show that the lift coefficients and the A/D are related and that this relationship depends on $\hat{f}$. These results were used in the VIVANA Theory Manual, (Larsen et al., 2005), to derive a lift coefficient model shown in Figure 3. The C_L versus A/D curve is defined by three points, A, B, and C, and the positions of these points are functions of $\hat{f}$. SHEAR7, (Vandiver et al., 2005), also uses this lift coefficient model to predict VIV. Using an iterative process and Equation 14 the amplitude and associated lift coefficient can be found by balancing the energy transfered from the fluid to the cylinder and the energy dissipated energy from mechanical damping. The maximum amplitude for an undamped cylinder under lock-in conditions corresponds to the A/D value for zero lift, which is point C in Figure 3. The work of Govardhan & Williamson (2006) indicates that the A/D value increases with increasing Reynolds number. This work show similar results for lift coefficients of flexible cylinders.

7 Conclusions

The non-dimensional frequency shows a change with respect to the Reynolds number, changing from 0.22 at Reynolds number 10^3 to 0.14 at Reynolds number 10^5. The amplitude of vibration, regardless of mode number, increases with increased Reynolds number. An open question is whether this dependence on Reynolds numbers holds for Reynolds numbers greater than 10^5; one experiment is shown with data up to 25000 and it fits the trend.

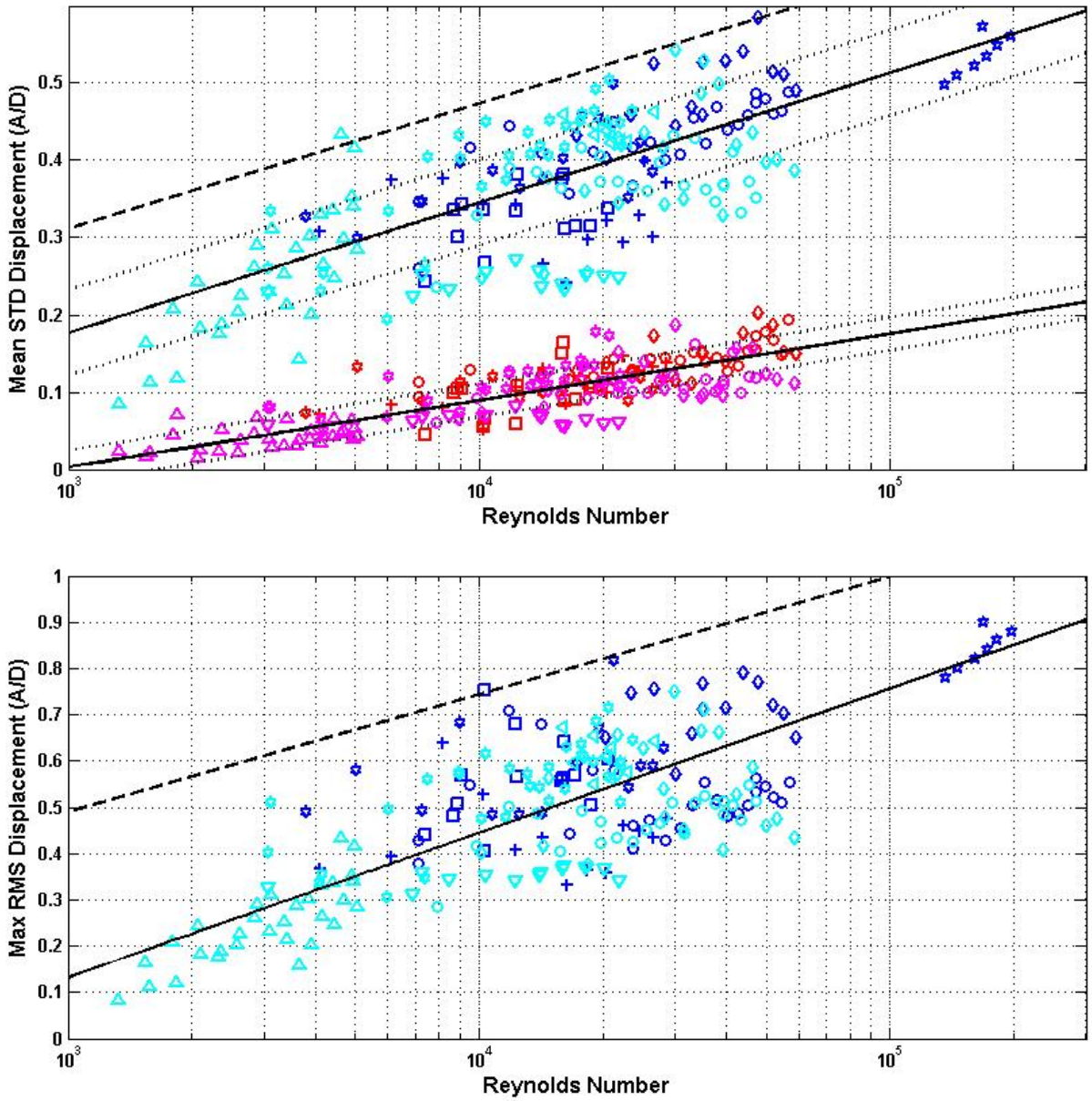

Figure 2. (top) The mean RMS amplitude $\left(\overline{\sigma}_{(y/D)}\right)$ divided by diameter is defined by Equation 6 plotted versus Reynolds Number. (bottom) The maximum RMS A/D for the cross-flow direction plotted versus Reynolds number. The symbols for the different tests are defined in Table 1.

A complex relationship exists between A/D, the non-dimensional frequency and the Reynolds number. Further research is needed to determine the controlling factor in the increase in amplitude.

8 Acknowledgments

The funding for this work was provided by the Center for Ship and Ocean Structures at NTNU. The authors would like to acknowledge the following groups for the use of their data in this analysis: NorskHydro for the Hangøytangen data; DeepStar and the MIT SHEAR7 JIP for the Gulf Stream and Lake Seneca Data; Statoil for the Steel Catenary Riser Data; The Norwegian Deepwater

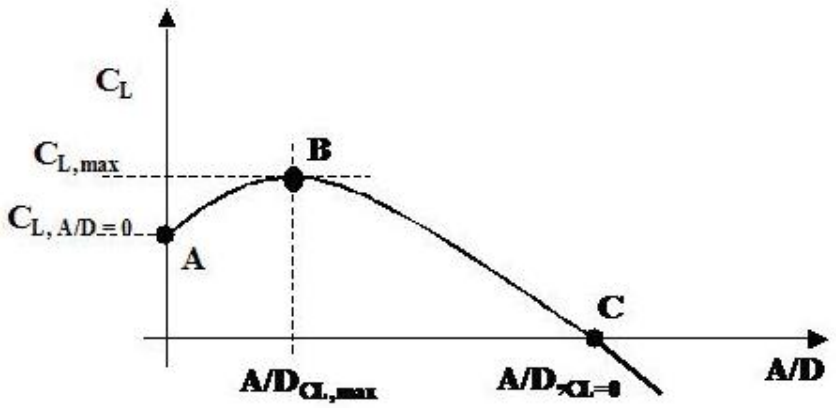

Figure 3. The lift coefficient model derived for VIVANA in Larsen et al. (2005).

Project (NDP) for the NDP High Mode Number Data and the Fairing Tow Tests; Exxon Production Research for the use of the Long Tensioned Riser Tests; and MIT and the SHEAR7 JIP for the Rotating Rig Data. Also special thanks to Prof. Charles Williamson of Cornell University for sharing his work, insight, and data with us.

9 Nomenclature

A - amplitude [m]
c - phase velocity [m/s] C - damping constant [kg/s]
C_L - lift coefficient [-]
D - diameter [m]
f - frequency [Hz]
$\hat{f}$ - non-dimensional frequency [-]
f_v - frequency of vibration [Hz]
K - spring force per unit displacement [N/m]
k - wavenumber [$1/m$]
m - mass per unit length [kg/m]
m* - mass ratio [-]
n - mode number [-]
R - R is the radial distance for the strain gauges [m]
Re - Reynolds Number [-]
U - current velocity [m/s]
V_{rn} - reduced velocity [-]
υ - kinematic viscosity [m^2/s]
ρ_f - fluid density [kg/m^3]
$\overline{\sigma}_{(y/D)}$ - mean RMS of displacement [-]
ω - frequency [rad/s]

REFERENCES

BLEVINS, R. D. 2001 *Flow-Induced Vibrations 2nd Edition*, Kriger Publications Co., 2001

BRAATEN, H., LIE, H. & SKAUGSET, K. 2008 Higher Order Modal Instability of Riser Fairings *Offshore Mechanics and Arctic Engineering Conference Lisbon June 2008* OMAE2008-57971.

BEARMAN, P. W. 1984 Vortex Shedding from Oscillating Bluff Bodies *Annual Rev Fluid Mechanics* **16** 195-222

GOPALKRISHNAN, R. 1993 Vortex-Induced Forces on Oscillating Bluff Cylinders *PhD Thesis, MIT Department of Ocean Engineering*

GOVARDHAN, R. & WILLIAMSON, C. H. K. 2000 Modes of Vortex formation and frequency response of a freely vibrating cylinder *J. Fluid Mech.* **420**, 85–130.

GOVARDHAN, R. N. & WILLIAMSON, C. H. K. 2006 Defining the 'modified Griffin plot' in vortex-induced vibrations: revealing the effect of Reynolds number using controlled damping. *J. Fluid Mech.* **561**, 147–180.

HALSE, K. H., KNUT, M. & LIE H. 1999 Vortex-Induced Vibrations of a Catenary Riser. *Third International Symposium on Cable Dynamics, Trondheim Norway, August 1999*

HUSE, E., KLEIVEN, G., & NIELSEN, F. G. 1998 Large scale model testing of deep sea risers. *Offshore Technology Conference Houston TX, May 1998* OTC-8701

KHALAK, A. & WILLIAMSON, C.H.K. 1997 Fluid forces and dynamics of a hydroelastic structure with low mass and damping *J. Fluid and Structures* **11**, 973–982.

LARSEN, C.M., VIKESTAD, K., YTTERVIK, R., PASSANO, E. & BAARHOLM G.S. 2005 VIVANA - Theory Manual Version 3.4 *Marintek Report 516419.02.01*

LIE, H. & KAASEN, K. E. 2006 Modal analysis of measurements from a large-scale VIV model test of a riser in lineared flow. *J. Fluid and Structures* **22**, 557-575.

LIE H., MO, K., & VANDIVER J. K. 1998 VIV model test of a bare- and a staggered buoyancy riser in a rotating rig *Offshore Technology Conference Houston TX, May 1998* OTC-8700.

MARCOLLO, H., CHAURASIA, H., & VANDIVER J. K. 2007 Phenomenon Observed in VIV Bare Riser Field Tests. *Offshore Mechanics and Arctic Engineering Conference San Diego CA 10-15 June 2007* OMAE2007-29562.

MAZEL, C. 1976 Vortex-excited vibrations of marine cables *Masters Thesis, MIT Department of Ocean Engineering*

SARPKAYA, T. 2004 A critical review of the intrinsic nature of vortex-induced vibrations *J. Fluid and Structures* **19**, 389-447.

SWITHENBANK, S. B. 2007 Dynamics of Long Flexible Cylinders at High-Mode Number in Uniform and Sheared Flows. *PhD Thesis, MIT Department of Mechanical Engineering*

TROPEA, C., YARIN, A., & FOSS, J. (EDITORS) 2007 *Springer Handbook of Experimental Fluid Mechanics*, Springer, 2007

TRIM, A. D., BRAATEN, H., LIE, H., & TOGNARELLI, M. A. 2005 Experimental investigation of vortex-induced vibration of long marine risers. *J. Fluid and Structures* **21**, 335-361.

VANDIVER, J. K. 1993 Dimensionless Parameters Important to the Prediction of Vortex-Induced Vibration of Long, Flexible Cylinders in Ocean Currents. *J. Fluid and Structures* **7**, 423-455.

VANDIVER, J. K. 1983 Drag Coefficients of Long Flexible Cylinders. *Offshore Technology Conference Houston TX, May 1983* OTC-4490.

VANDIVER, J.K, LEE, L., LEVERETTE, S., & MARCOLLO, H. 2005 User Guide for SHEAR7 Version 4.4 *MIT*

VANDIVER, J. K., MARCOLLO, H., SWITHENBANK, S. B. & JHINGRAN V. 2005 High-Mode Number Vortex-Induced Vibration Field Experiments. *Offshore Technology Conference Houston TX, 2-5 May 2005* OTC-17383.

VANDIVER, J. K., SWITHENBANK, S. B., JAISWEL, V. & JHINGRAN V. 2005 Fatigue Damage from High-Mode Number Vortex-Induced Vibration. *Offshore Mechanics and Arctic Engineering Conference Hamburg Germany 4-9 June 2006* OMAE2006-9240.

VIKESTAD, K., LARSEN, C. M. & VANDIVER, J. K. 2000 Norwegian Deepwater Program: Damping in Vortex-Induced Vibrations *Offshore Technology Conference Houston TX, May 2000* OTC-11998.